Interferometric imaging by deconvolution: theory and numerical examples

Ivan Vasconcelos and Roel Snieder†
† *Center for Wave Phenomena, Colorado School of Mines, Golden, CO 80401, USA*

Summary

Seismic interferometry is a field of growing interest in exploration seismology. In this paper we provide the theoretical basis for performing interferometry by deconvolution. We argue that for general models, deconvolution interferometry gives only the causal scattering response between any two receivers, as opposed to cross-correlation which gives both causal and acausal scattering responses. Deconvolution interferometry also gives rise to a spurious event not present in cross-correlation. Through a simple model, we gain physical insight about the meaning of each term in deconvolution interferometry. We also show deconvolution interferometry can also be accomplished after summation over sources. We demonstrate the feasibility of deconvolution interferometry with numerical examples on with impulsive sources, and show that the deconvolution interferometry artifacts are not mapped onto the image space. Finally, we show that deconvolution interferometry can successfully image drill-bit source data without independent estimates of the source function with quality comparable to impulsive source data.

Introduction

Seismic interferometry consists in extracting the Green's function between two receivers by correlating the wavefields recorded at these two receivers, excited by incoherent sources. Different proofs on how Green's functions emerge from correlations are available in the literature: by representation theorems (Weaver and Lobkis, 2004), by time-reversal (Bakulin and Calvert, 2004), by stationary-phase analysis (Snieder et al., 2005) are just some examples.

In drill-bit seismic imaging, cross-correlated drill-bit noise shows a strong imprint of the drill-bit source function (Poletto and Miranda 2004). If this source imprint is not accounted for, the resulting SWD image could be uninterpretable. Deconvolution interferometry can potentially not only be a viable option to multidimensional interferometric imaging, but it may also prove to be a key technology in some applications, such as drill-bit imaging.

Deconvolution versus cross-correlation

Let the frequency-domain wavefield $u(\mathbf{r}_A, \mathbf{s}, \omega)$ recorded at $\mathbf{r}_A$ be the superposition of the impulsive direct and scattered wavefields $u_0(\mathbf{r}_A, \mathbf{s}, \omega)$ and $u_S(\mathbf{r}_A, \mathbf{s}, \omega)$ convolved with a source function $S_s(\omega)$ associated with an excitation at $\mathbf{s}$. It is important to note here that the wavefields $u(\mathbf{r}_A, \mathbf{s}, \omega)$ may be elastic and attenuative, and $u_S(\mathbf{r}_A, \mathbf{s}, \omega)$ may contain higher-order scattering and inhomogeneous waves. Also, $S_s(\omega)$ can be arbitrarily complex, and may vary as a function of $\mathbf{s}$. Given that the deconvolution of a wavefield recorded at $\mathbf{r}_A$ by another recorded at $\mathbf{r}_B$ is represented by D_{AB}, then to perform interferometry by deconvolution it is necessary to integrate D_{AB} over some closed surface Σ containing the sources:

$$\int_\Sigma D_{AB}(\omega)\, d\mathbf{s} = \int_\Sigma \frac{u(\mathbf{r}_A, \mathbf{s}, \omega) u^*(\mathbf{r}_B, \mathbf{s}, \omega)}{|u(\mathbf{r}_B, \mathbf{s}, \omega)|^2}\, d\mathbf{s}\,, \quad (1)$$

where * denotes complex-conjugation. It follows form right-hand side of equation [1] that the source function $S_S(\omega)$ gets canceled in the integrand. As in the cross-correlation approach (Snieder et al., 2006), the numerator in equation [1] is not zero-phase and expands to four wavefield cross-terms from recordings at $\mathbf{r}_A$ and $\mathbf{r}_B$. The denominator is strictly zero-phase, but it is oscillatory and contains cross-terms between the scattered and direct wavefields at $\mathbf{r}_B$. To identify the leading order terms in equation [1] we assume $|u_0|^2 >> |u_S|^2$ to drop terms which are quadratic on scattered wavefields. The denominator can be factored in $|u_0(\mathbf{r}_B, \mathbf{s}, \omega)|^2$, then we expand it first-order Taylor series. When multiplying the numerator by the expansion of the denominator we again ignore terms quadratic in scattering, which leads us to

$$\begin{aligned}\int_\Sigma D_{AB}(\omega)\, d\mathbf{s} = & \underbrace{\int_\Sigma \frac{u_0(\mathbf{r}_A, \mathbf{s}, \omega) u_0^*(\mathbf{r}_B, \mathbf{s}, \omega)}{|u_0(\mathbf{r}_B, \mathbf{s}, \omega)|^2}\, d\mathbf{s}}_{D1} \\ & + \underbrace{\int_\Sigma \frac{u_S(\mathbf{r}_A, \mathbf{s}, \omega) u_0^*(\mathbf{r}_B, \mathbf{s}, \omega)}{|u_0(\mathbf{r}_B, \mathbf{s}, \omega)|^2}\, d\mathbf{s}}_{D2} \\ & - \underbrace{\int_\Sigma \frac{u_S(\mathbf{r}_B, \mathbf{s}, \omega) u_0(\mathbf{r}_A, \mathbf{s}, \omega) u_0^*(\mathbf{r}_B, \mathbf{s}, \omega)}{u_0(\mathbf{r}_B, \mathbf{s}, \omega)}\, d\mathbf{s}}_{D3}\,, \quad (2)\end{aligned}$$

which shows the three leading-order terms in performing deconvolution interferometry before stacking over sources. Note that if $u_0(\mathbf{r}_B, \mathbf{s}, \omega)$ is comprised of a single impulsive arrival, the oscillatory character of integrands in $D1$ and $D2$ (equation [2]) is due to the behavior of the numerators alone. This turns our attention back to interferometry by cross-correlations. Assuming a source function $S(\omega)$ that is slowly-varying with $\mathbf{s}$, then

$$\begin{aligned}\int_\Sigma C_{AB}(\omega)\, d\mathbf{s} &= \int_\Sigma u(\mathbf{r}_A, \mathbf{s}, \omega) u^*(\mathbf{r}_B, \mathbf{s}, \omega)\, d\mathbf{s} \\ &\approx |S(\omega)|^2 \left(C1 + C2 + C3 + C4\right)\,, \end{aligned} \quad (3)$$

where $C1$ through $C4$ are the same cross-terms as for the numerator in the integrand of equation [3], respectively: direct-direct†, scattered-direct†, direct-scattered† and scattered-scattered†. In correlation interferometry, the term $C2$ gives rise to a causal response corresponding to $u_S(\mathbf{r}_A, \mathbf{r}_B, \omega)$ (Snieder et al.,

† - this is used to denote time-reversal. The terms associated with the deconvolution/correlation filters are time-reversed.

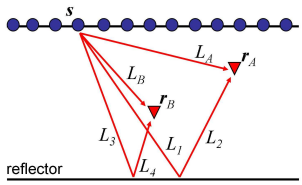

Fig. 1: This model can be used to gain intuitive understanding about the physical meaning of the terms in equation [2]. receivers are imbedded in an acoustic homogeneous half-space containing a single reflector, bounded by a perfectly absorbing surface. Only direct and single-scattered waves are considered. Sources are depicted by circles on the surface, the two receivers are represented by triangles. L_A, L_B and L_1 through L_4 are the lengths of the corresponding ray segments. The reflection coefficient r is constant with respect to both position and incidence angle.

2006), the scattered wavefield as if the source were located at $\mathbf{r}_B$. $C3$ gives a response that corresponds to $u_S^*(\mathbf{r}_A, \mathbf{r}_B, \omega)$. The terms $C1$ and $C4$ are respectively associated with causal and acausal $u_0(\mathbf{r}_A, \mathbf{r}_B, \omega)$.

By inspecting equation [2], we observe that the phase in the integrand of $D1$ is equal to that of $C1$ in equation [3]. The same relationship holds between $D2$ and $C2$. $C3$ and $C4$ have no corresponding terms in equation [2]. These remarks have an important consequence: interferometry by deconvolution of receiver gathers will only provide the causal scattering response as if the excitation occurred at the receiver that acts as the deconvolution filter. This holds regardless of medium properties or acquisition geometry. It also holds if integration over sources is not conducted over a closed surface, as long as there are sources that lie in the stationary path connecting the integration surface, the receivers and the scatterers. Integration over a non-closed surface yields artifacts in interferometric data if the medium is inhomogeneous (Snieder et al., 2006).

The term $D3$ in equation [2] gives rise to a spurious event that does not correspond to any physical phenomena that would occur if there were a physical source sitting at one of the receivers. The minus sign in front of $D3$ in equation [2] shows that this term will appear with a polarity that is opposite with respect to the other two terms. Albeit being unrelated to physical wavefield events, the term $D3$ does have a physical meaning which we will discuss in a later section of this paper.

Physical insight from a simple model

The objective of this section is to simplify our problem by means of evaluating the each term in equation [2] separately for the model specified in Figure 1. By representing $u_{0,S}(\mathbf{r}_A, \mathbf{s}, \omega)$ and $u_{0,S}(\mathbf{r}_B, \mathbf{s}, \omega)$ through the acoustic far-field Green's functions according to the ray-lengths in Figure 1, we can rewrite each term in equation [2] as for instance:

$$D1 = \frac{1}{(4\pi L_B)^2} \int \frac{e^{ik(L_A - L_B)}}{L_A L_B} dxdy \ , \qquad (4)$$

We then evaluate these integrals using the zero-order stationary phase method to determine the asymptotic approximation for each term. For $D1$ (equation [4]), the stationary-phase condition requires the source to be in the stationary of the direct wave between the two receivers, and the integral evaluation yields exactly the traveltime of a direct arrival that propagates from $\mathbf{r}_B$ to $\mathbf{r}_A$. The stationarity condition pertaining to term $D2$ states the stationary source point is on the path of the arrival that departs from $\mathbf{r}_B$, bounces off the reflector and is recorded at $\mathbf{r}_A$. The asymptotic form of the term $D3$ cannot be expressed in terms of the Green's functions between $\mathbf{r}_A$ and $\mathbf{r}_B$.

Another advantage arises from specifying a model such as in Figure 1 lies in the fact that we can actually compute the phases of the integrands for both cross-correlation and deconvolution gathers (C_{AB} and D_{AB} for all shot points). As we will demonstrate with numerical examples, this allows us to establish a correspondence between events in the deconvolution/cross-correlation gathers with events in the interferometric shot gathers.

Deconvolution after summation over sources

In order to suppress the influence of the source pulse that remains after interferometry by cross-correlations (equation [3]), deconvolution can be applied after summation over sources in the following manner:

$$\frac{\int_\Sigma C_{AB}(\omega)\, d\mathbf{s}}{\int_\Sigma C_{AB}(\omega)\, d\mathbf{s}} \quad \approx \quad (C1 + C2 + C3 + C4) \ , \qquad (5)$$

plus terms quadratic on scattering. C_{BB} is the autocorrelation of the wavefield recorded at $\mathbf{r}_B$. This result was obtained in a sequence of two steps. First we derived the denominator into four terms that contain the power spectra of $u_0(\mathbf{r}_B, \mathbf{s}, \omega)$ and $u_S(\mathbf{r}_B, \mathbf{s}, \omega)$ and cross-terms direct-scattered† and scattered-direct†. Here, we also assume a slowly-varying source pulse $S(\omega)$. The second step is analogous to the derivation of equation [2], where we assume $|u_0|^2 >> |u_S|^2$, and then expand the denominator on the left-hand side of equation [5] to first-order. To leading order, equation [5] carries essentially the same four terms as interferometry by cross-correlation (equation [3]), except the power spectrum of the source is no longer present.

Numerical modeling

The model used for the examples portrayed here was composed of a water layer with a wavespeed of 1500 m/s. A flat, horizontal interface was placed at 2500 m depth. The receivers were positioned in a horizontal line at 750 m depth, starting at lateral position $x =$ 1500m and ending at 3000 m, with increments of 25 m. The source line was also horizontal at a depth of 400 m, ranging from $x = 500$ m to 4500 m, with increments of 50 m. The data was modeled by 2D acoustic finite-differencing with absorbing boundary conditions.

Impulsive source data

In this paper, by the use of the term "impulsive source" we refer to any pulse that has the character of a band-limited delta distribution. The data for this example was in fact modeled with a second-derivative Gaussian pulse of 5 Hz peak frequency.

Figure 3a,b show deconvolution and cross-correlation gathers computed from the last and first (used as filter) receiver gathers. Figure 3a confirms the presence

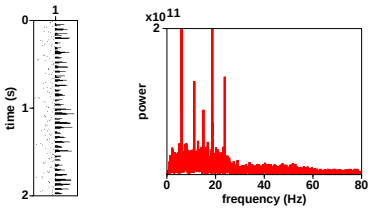

Fig. 2: Modeled drill-bit source function and spectrum. Here we chose to display the first 2 s of the total 45 s of the modeled pulse.

of the leading order terms highlighted in equation [2], and it is supported by the ray-theoretical traveltimes for the three terms described by equations as in [4]. The acausal $C3$ term and the $C4$, seen in Figures 3c,d indeed are not present in the deconvolution gathers.

The interferometric (virtual) shot gathers for deconvolution before source stack, cross-correlation, and deconvolution after source stack are shown in Figure 4. Causal and acausal direct arrivals can be seen in all three gathers. The causal primary reflection event can also be identified in all gathers, arriving at approximately 2.5 s at zero-offset. The acausal primary is only present in (b) and (c). The spurious event introduced by the term D3 (equation [2]; Figure 3a,b) appears in Figure 4, with the same zero-offset traveltime as the primary reflection, but with opposite polarity and with a slower move-out character. Since deconvolution interferometry strictly requires the zero-offset trace to be a spike at $t = 0\,\mathrm{s}$ (Figures 4a,c) and zero at all other times, spurious events with opposite polarity are generated to cancel the contribution of physical events at the zero-offset trace for non-zero times. The spurious events are a consequence of this additional boundary condition imposed on the data.

The images (Figure 5) obtained from shot-profile wave-equation migration the gathers in Figure 4 pose an encouraging scenario for the practice of interferometry. First, all three images map the energy at the correct subsurface locations. Second, the similarity between all three images shows that the spurious event ($D3$) in Figure 4a vanishes in the image domain. This happens because the imaged depth of the spurious arrival is varies with receiver-receiver offset. Hence, for the example of common-offset imaging the stack of different offset images of the spurious event adds destructively in the final image, whereas physical events add constructively. Note that through all impulsive source examples, deconvolution interferometry compresses the source pulse with respect to cross-correlation interferometry.

Drill-bit source data

Drill-bit noise records are characterized by a continuous noise source that is dominated by certain specific frequencies (Poletto and Miranda, 2004). This poses a problem for cross-correlation interferometry because interferometric gathers would be dominated the source spectrum (equation [3]). In typical drill-bit application this problem is overcome by placing accelerometers on the drill-stem as an estimate of the drill-bit source function. Deconvolution interferometry provides a new option to the processing of drill-bit seismic data, specially if the accelerometer records are not available. Our model was designed to replicate the drilling characteristics of a tricone drill-bit dominated by the characteristic frequencies of the teeth indentation, trilobe pattern, mud-pump strokes, and composite vibrations (Poletto and Miranda, 2004). Figure 2 shows a portion of the modeled drill-bit source pulse, and the source spectrum.

The drill-bit interferometric shot gathers obtained from deconvolution and correlation are shown respectively in Figures 6a,c. The reflection event is clearly visible in the deconvolution shot gather, whereas in the correlation shot gather it cannot be identified. The migrated images in Figures 6b,d show that the deconvolution interferometric image of drill-bit data is of comparable quality to the impulsive shot images in Figure 5. The correlation-based interferometric image of the drill-bit data carries the signature of the source spectrum. Note that Figure 6 also shows the effect of migration as a de-noising procedure.

Conclusions

By representing recorded wavefields as a superposition of direct and scattered wavefields, we derived the leading-order terms that follow from performing deconvolution interferometry on receiver gathers before summing over sources. This derivation suggests that interferometry by deconvolution before stacking over sources yields only the causal term related to the scattered wavefield as if one of the receivers were a virtual source. A spurious term of leading order arises in deconvolution interferometry. Through a simple toy model we were able to evaluate asymptotic approximations to the terms in deconvolution interferometry using the stationary-phase method. We also argued that interferometry can also be accomplished by deconvolution after summation over sources, which would yield terms analogous to correlation-based interferometry.

Numerical examples with impulsive source data showed deconvolution interferometry can successfully retrieve the causal response between two receivers. This response can be used to build interferometric shot gathers which in turn can be imaged. Imaging of deconvolution interferometric shot gathers proved to practically eliminate the spurious arrival generated by the deconvolution method. In the case of a drill-bit source, deconvolution interferometry proved to be able to properly image the subsurface structure without the need for an independent estimate of the source pulse (e.g., drill-stem accelerometer). This cannot be accomplished by correlation-based interferometry.

References

Bakulin, A. and Calvert, R., 2004, Virtual source: new method for imaging and 4D below complex overburden: Soc. Expl. Geophys., Expanded Abstracts, 2477–2480.

Poletto, F., and Miranda, F., 2004, *Seismic While Drilling - Fundamentals of Drill-Bit Seismic for Exploration*: Monograph, Elsevier Ltd., United Kingdom, 520 pages.

Snieder, R., Wapenaar, K. and Larner, K., 2005, Spurious multiples in seismic interferometry of primaries: CWP Project Review book, CWP-500P.

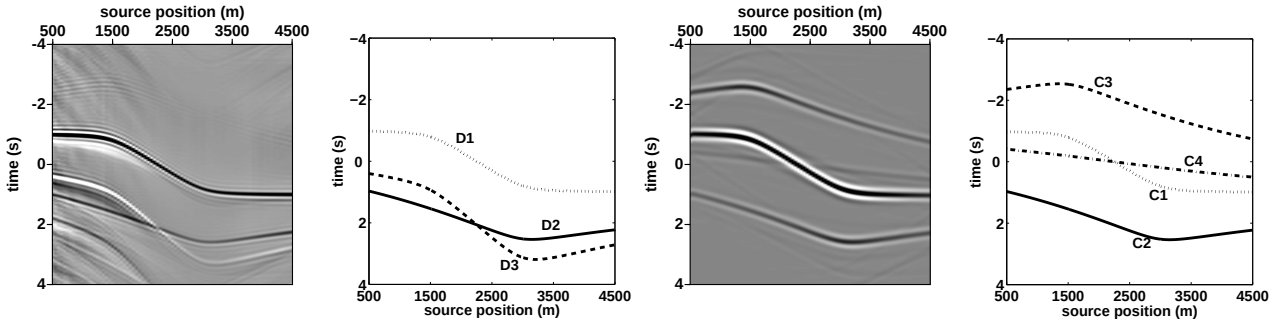

(a) (b) (c) (d)

Fig. 3: Deconvolution and cross-correlation gathers for the first and last receivers, whose lateral positions are, respectively, 1500 and 3000 m. (a) displays the deconvolution gather obtained from deconvolving the modeled common-receiver gathers, whereas (b) shows ray-theoretical traveltimes for the terms in equation [2], computed according to equations as in [4]. Analogous to (a), (b) is the cross-correlation gather generated from source-by-source correlation of the two receiver gathers. (c) shows the asymptotic traveltimes corresponding the phase of the integrands in equation [3].

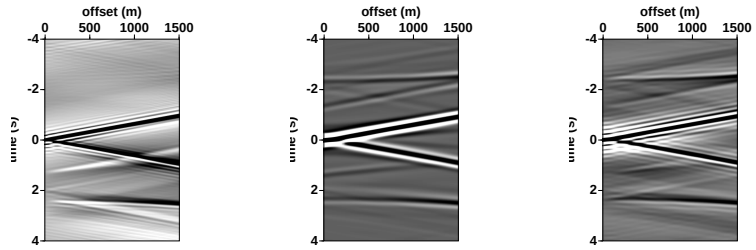

(a) (b) (c)

Fig. 4: Virtual (interferometric) shot gathers with the virtual shot positioned at the receiver at 1500 m. The gather in (a) is obtained by deconvolution before stacking (equation [1]), (b) is generated by simple cross-correlations (equation [3]) and (c) is done by deconvolution after summation over sources (equation [5]).

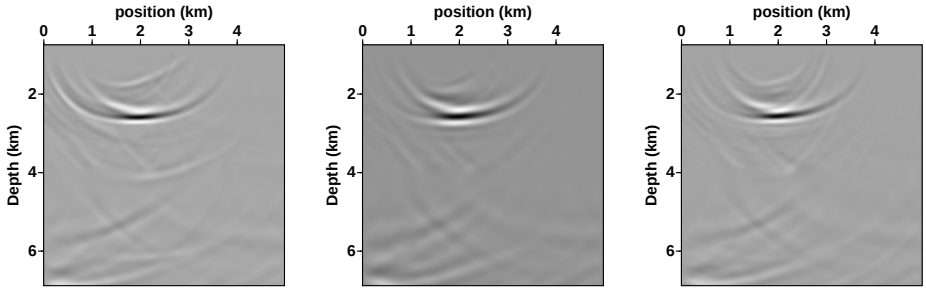

(a) (b) (c)

Fig. 5: Shot-profile wave-equation migrated images of the virtual shot gathers in Figure 4. In this figure, (a), (b) and (c) are the images obtained from migrating the gathers in Figure 4a, b and c, respectively. The true depth of the target interface is 2500 m.

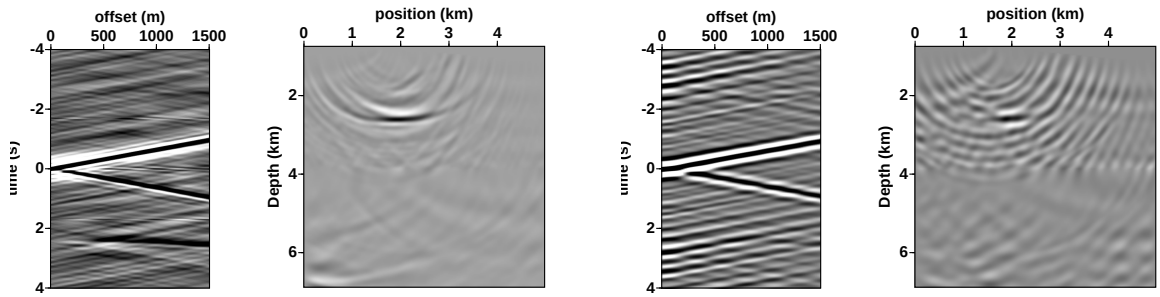

(a) (b) (c) (d)

Fig. 6: Virtual shot (receiver at 1500 m) for the drill-source data computed by deconvolution before stack (a), and by cross-correlation (c). (b) is the result of shot-profile wave-equation imaging of (a), whereas (d) is the shot-profile image of (c).